In-situ High-Resolution Transmission Electron Microscopy and X-ray Diffraction Studies on Nanostructured *β*-SiC and Its Promising Feature for Photocatalytic Hydrogen Production

IOP Conf. Series: Materials Science and Engineering **515** (2019) 012012 doi:10.1088/1757-899X/515/1/012012

In-situ High-Resolution Transmission Electron Microscopy and X-ray Diffraction Studies on Nanostructured *β*-SiC and Its Promising Feature for Photocatalytic Hydrogen Production

Nurul Hidayat[1,*], Abdulloh Fuad[1], Nandang Mufti[1], Ummu Kultsum[1], Anggun Amalia Fibriyanti[1], Sunaryono[1], Bambang Prihandoko[2]

[1] Department of Physics, Faculty of Mathematics and Natural Sciences, Universitas Negeri Malang, Jl. Semarang 5, Malang 65145, Indonesia
[2] Research Center for Physics, Indonesian Institute of Sciences (LIPI), Kawasan PUSPITEK Serpong, Banten 15310, Indonesia

*Corresponding author's email: nurul.hidayat.fmipa@um.ac.id

Abstract. The ruin of energy and environmental pollution has led to the pursuit of novel technologies for green energy productions. For hydrogen energy itself, the search for the photocatalytic-based nanostructured *β*-SiC is one of the main research focus during the last few years. Herein, we reported the successful magnesiothermic reduction at low temperature, i.e., 700 °C, using an argon gas tubular furnace to fabricate *β*-SiC with a particle size below 10 nm. The X-ray diffraction (XRD) data collection and Rietveld refinement showed the single phase of moissanite *β*-SiC formation having cubic structure with lattice constants of $a = b = c = 4.3523(50)$ Å and $\alpha = \beta = \gamma = 90°$. The formation of the nanostructured *β*-SiC was well confirmed by the high-resolution transmission microscopy (HRTEM) image. The equivalent crystallite size produced by the XRD profile analysis was 4.2(8) nm, and extracted from the HRTEM image was about 6 nm. The *d*-spacing for (111) plane met a reliable agreement between the XRD and HR-TEM data. The energy dispersive X-ray spectroscopy in scanning transmission electron microscopy (STEM-EDS) also brought a good capture for the nearly 50:50 concentration of Si:C in our sample. Furthermore, in-situ heating experiments via HR-TEM were also conducted. In brief, carbon nanolayers were initiated on the surface of the nanostructured *β*-SiC. All these fine-tuned crystallographic properties assigned the as synthesized *β*-SiC to be the promising candidate for photocatalytic hydrogen production.

Keywords: Nanostructured *β*-SiC, Rietveld refinement, in-situ HR-TEM, hydrogen production

1. Introduction

We dream for a future where the planet we live in, the Erath, serves us with its best fresh air and where the industries are sustainable and clean. The best endeavor is to support the construction of power sources that eliminate pollution. Hydrogen production and full cell systems, for example, are claimed to have superior performances to replace nonrenewable hydrocarbon fuels [1,2]. Many attempts have been continuously made to optimize the performance of hydrogen production and fuel cell technologies [3–6]. Development of photocatalytic materials for water splitting turns out to be the supreme breakthrough to

hydrogen production advancement due to the abundant of solar light and the renewability of water resources [7].

Recent studies explored the role of photocatalytic water splitting for hydrogen production using *β*-SiC [7–9]. This cubic structure of SiC, identified as *β*-SiC, is preferable than other polytypes of SiC. Although *α*-SiC is as powerful as *β*-SiC regarding its chemical and thermal stabilities, producing controlled cubic structured *β*-SiC is easier than the *α*-SiC which crystallizes in hexagonal structure [10]. Only one cubic crystal system does SiC have wherein there exist three double-layers of Si-C of the lattice stacking periodicities, and, hence, it is well known as 3C-SiC or *β*-SiC. The other Si-C stacking arrangements formed hexagonal and rhombohedral structures. Hexagonal SiC that has 6 and 4 Si-C double-layers, for example, are respectively recognized as 6H-SiC and 4H-SiC. The SiC properties are determined by its Si-C double-layers arrangements [11]. Thus, it is important to have good control, constructively, on the synthesized SiC.

Numerous approaches have been achieved for fabricating and exploring the properties of *β*-SiC nanomaterials; some examples are given as follows. *β*-SiC nanospheres have been prepared via Terbium-catalyzed carbothermal reduction at 1200-1300 °C [12]. Microwave-assisted thermal evaporation using 1650–1750 °C [13], carbothermal reduction at 1500 °C [14], hot wire chemical vapor deposition with filament temperature of 2000 °C [15], combined method of carbothermal reduction and sol-gel impregnation employing two-step heating (using Ar gas furnace at 1050 °C followed by 1550 °C heat treatments) [16], high-frequency induction using heat treatment at 1800 °C [17], and arc plasma heating at 3000 °C [18] were conducted to produce nanostructured *β*-SiC. However, the temperatures are still relatively high which give rise to synthesis expense and efficiency. In this present study, we report the establishment of magnesiothermic reduction approach for nanostructured *β*-SiC preparation. The magnesiothermic route relies on the SiO_2 chemical bond breaking mechanism at lower temperatures, and it controls the arrangements of silicon carbide stacking arrangements [19].

The performances of nanosized crystals extensively depend on their atomic structures. Nanoparticles, having nanoscale size and high surface area, demonstrate unique characteristics, and they are often significantly much more exclusive than those of the bulk polycrystalline materials [20]. As a result, XRD diffraction alone, for the detailed crystal structure analysis, is never enough to convey the fundamental nature of the crystalline characteristics of nanosized materials. Hence, a deeper investigation into the crystalline state of matter is required. Herein, we accomplished that via HR-TEM characterization to observe the lattice arrangements and to support the Rietveld crystal structure analysis. The fine-controlled *β*-SiC nanostructure will meet the criteria for photocatalytic materials for water splitting technologies.

2. Methods

In this present study, highly purified nano silica SiO_2, from a previous report [21], was wisely ground with $C_{12}H_{22}O_{11}$. Precise quantities of H_2SO_4 and distilled water were added to the $SiO_2/C_{12}H_{22}O_{11}$ mixture powder followed by six hours heating at 100 °C and elevated to 160 °C for the succeeding six hours. The heated powder underwent one-hour carbonation at 700 °C in an argon gas tubular furnace to decompose carbon from $C_{12}H_{22}O_{11}$ which in turns forming SiC/C product. The composite was added by Mg powder and heated at 800 °C for 18 h at the same furnace costumed setting. The *β*-SiC crystal was further favorably accomplished by three-hour leaching process using HF and HNO_3 solutions, which was designed for removing magnesium oxide and silicon dioxide impurities, using a hot plate with stirring speed of 600 rpm at 100 °C. Filtrating and cleaning were conducted with distilled water for 30 minutes. For detailed structural characterization purposes, X-ray diffraction (XRD) and high-resolution transmission electron (HR-TEM) microscopy, integrated with energy dispersive X-ray spectroscopy in scanning transmission electron microscopy (STEM-EDS) were employed.

The CuKα XRD (X'Pert Pro-Panalytical) was benefitted using 40 kV and 30 mA electrical setting. The divergence slit was fixed for continuous scanning. The as-produced SiC was characterized by the XRD from 10° to 80° with a step angle of 0.02 and scan step of 0.5 s. The recorded XRD pattern was matched by the appropriate phase model prior to Rietveld refinement analysis to reveal the SiC crystal

structure properties. The Rietveld refinement was run by Rietica software [22]. Scale factor was the first parameter to refine followed by using polynomial 5th order backgrounds and sample displace. The refinement of lattice parameter and atomic factors were conducted very carefully. In succession, the Voigt (How. Asym) peak shape was chosen to extract the equivalent particle size of the crystalline SiC. The Rietveld analysis was finished by refining the peak shape, including adjusting the preferred orientation for (111) Bragg plane using the March model. The Rietveld refinement can be accepted if and only if the calculated XRD pattern is well-fitted with the observed XRD pattern.

Modern remote controlled HR-TEM and STEM-EDS with sharp brightness, high beam current produced field emission gun, and the constant powered objective lens was fully loaded to capture the nanostructural characteristics of the SiC product. The information limit and resolution were set at 0.12 nm and 0.16 nm, respectively. The characterization was conducted at 200 kV with a minimum step size of 50 kV. The STEM-EDS chemical mapping was conducted at 700 °C, 1000 °C, and 1200 °C.

3. Results and Discussion

After successful XRD data collection and phase identification, a very careful Rietica assisted Rietveld refinement has been run to extract the full crystallographic properties of the as-synthesized *β*-SiC. The refinement output plot is depicted in Figure 1. The phase identification revealed that the only occurring crystalline phase in the sample, based on the XRD profile, was moissanite 3C-SiC, without any other impurities. Hence, all diffraction peaks of the measured XRD profile (denoted by circles) are entirely matched and fitted with the calculated profile (denoted by a solid line), as can be viewed in Figure 1. The XRD pattern displays the excellent character of the crystalline *β*-SiC. Such high purity of single *β*-SiC crystalline phase was also formed using a chemical vapor deposition method but higher temperatures, i.e., 1200-1400 °C [23]. The crystallographic data and Rietveld refinement report of the *β*-SiC can be attained from Table 1. The background is one of the most challenging parameters to deal with Rietveld refinement since it cannot be avoided. For any XRD pattern refinement, background gives many effects on the *R*-values [24]. As seen from Figure 1, the background displays polynomial function. That is why a polynomial fitting with five orders was chosen for background refinement fitting.

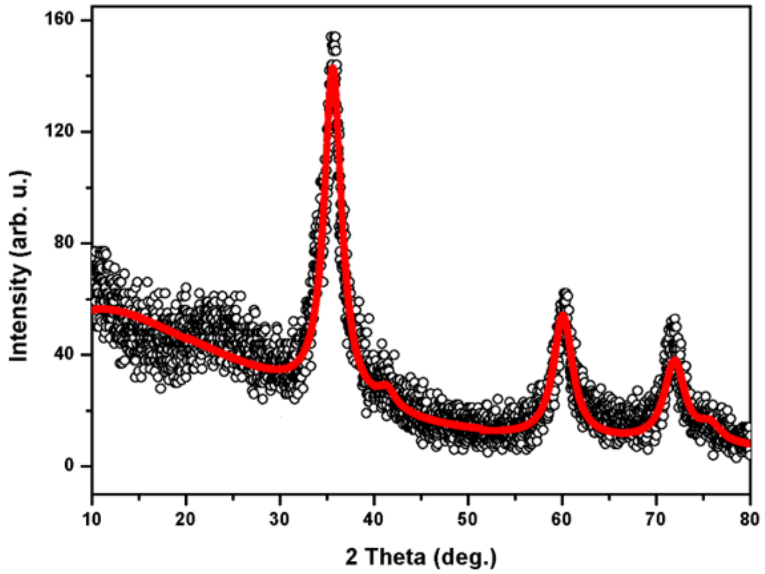

Figure 1. The Rietveld refinement output for the nanostructured *β*-SiC synthesized by the magnesiothermic approach. The circles and the solid lines respectively represent the measured and calculated XRD profile.

Table 1. Crystallographic parameters for the *β*-SiC from Rietica assisted Rietveld refinement. The numbers in parentheses represent the corresponding last digits of the estimated results.

Figure of Merits	R*p* (%)	12.05
	R*wp* (%)	15.04
	R*exp* (%)	17.10
	Gof (%)	0.77
Background	*B*-1	-451.43(26)
	*B*0	146.8(52)
	*B*1	-5.16(21)
	*B*2	0.069(30)
	*B*3	-0.00032(27)
Asymmetry	0.34(1)	
Sample Displacement	-0.13(2)	
Phase Scale factor	0.0097(5)	
Lattice Parameter (Å)	$a = b = c = 4.3523(50)$; $\alpha = \beta = \gamma = 90°$	
Space Group	*F -4 3 m*	
Cell Volume (Å^3)	82.44(19)	
Density (g/cm^3)	3.23	
Molecular Weight (amu)	160.39	
Derived Bragg *R*-factor	1.87	
Particle Size Equivalent (nm)	4.2(8)	

Table 2. Atomic positions of Si and C in the nanostructured *β*-SiC.

Atom	Type	Symmetry Multiplicity	*X*	*y*	*z*	Occupancy
Si	Si^{4+}	4*a*	0	0	0	0.0833
C	C^{4-}	4*c*	0.25	0.25	0.25	0.0833

The five background parameters are depicted in Table 1. Those are the parameters governing the background profile for the as-synthesized *β*-SiC. The asymmetry dictates the difference plot of sine-like shapes of XRD pattern. Notice that the asymmetry value is in the accepted value, less than one and more than zero. Compared to all refinement parameters, the phase scale factor influences the most on the figure of merits. The phase scale is 0.0097(5) indicating that there is a huge difference in height intensities between the calculated and measured XRD patterns. In this case, the *β*-SiC diffraction intensities are much lower than those of the *β*-SiC XRD model. This finding brings a sign of a small crystallite size compensation. The full width at half maximum (FWHM) values varies from 2.15° to 2.75°. Rietica enables the equivalent particle size calculation using the well-known Scherrer equation [25]. The equivalent particle size of *β*-SiC is below 10 nm, to be precise, it is 4.2(8) nm. In addition the lattice constants of the as-synthesized *β*-SiC are $a = b = c = 4.3523(50)$ (Å). It is very close to the lattice parameters of *β*-SiC reported by others [26–28].

From the crystallographic viewpoint, the silicon and carbon atoms comprising SiC crystals are joined by the strong covalent bond. The strong bonds of sp^3-hybridized tetrahedral sites empower every carbon or silicon atom to bind the other four nearest-neighbor silicons or carbons. This chemical interaction gives rise to the high performance of SiC to have outstanding thermal chemical and chemical stabilities. The SiC crystallographic profiles comprise of close-packed arrangements of bilayers of the atomic constituents. Among over 250 polytypes of SiC, due to the different silicon-carbon double layers, only a few of them are comprehensively explored [29]. Furthermore, *β*-SiC is one of the noblest polytypes which has not only seriously studied, but it has also been offering excellent performances in a wide range of applications [10,30].

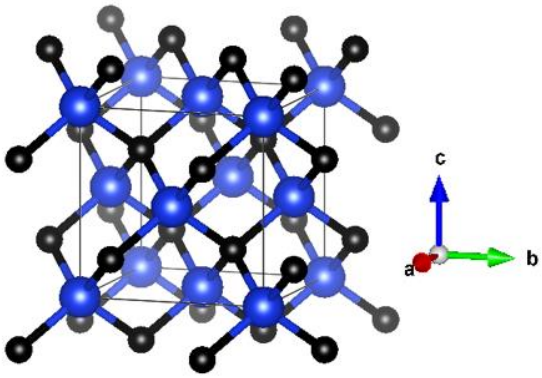

Figure 2. Crystal model of the as-produced nanostructured *β*-SiC. The blue and black spheres respectively represent silicon and carbon atoms.

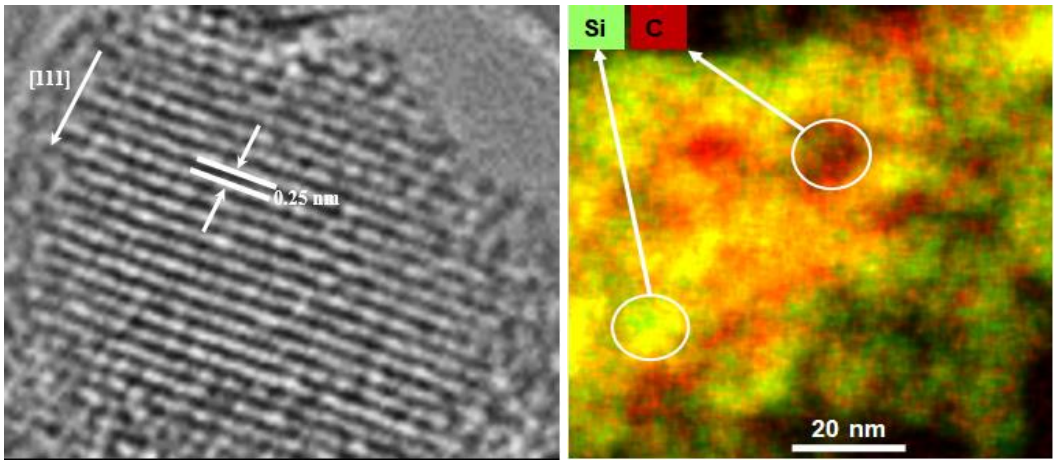

Figure 3. HR-TEM image at the [111] direction (left) and the elemental STEM-EDS mapping of the cubic nanostructured *β*-SiC prepared by magnesiothermic route.

Furthermore, the atomic sites of the nanosized *β*-SiC are given in Table 2. Being located at 4*a* and 4*c* Wyckoff positions for Si and C, respectively, they lie in specific atomic locations as tabulated in Table 2. Hence, from these crystallographic data, the crystal model for *β*-SiC, which is visualized using VESTA [31], a 3D visualization software for structural modeling, is captured in Figure 2. Visibly from Figure 2, the silicon atoms are located at the faces of the cube and the corner lattice points. All Si-C bilayers are arranged in the same orientation producing a zinc blende structure for *β*-SiC [32]. Our study confirmed that SiC exhibited tetrahedral molecular bonding with a central silicon atom surrounded equidistantly by four carbon atoms, or vice versa.

Figure 3 displays the lattice arrangements at [111] direction captured by HR-TEM and the elemental mapping with STEM-EDS. Using the STEM-EDS measurement for 8 minutes and screen current of 200 μA, the distribution of silicon (47.1 at%) and carbon (52.9 at%), which is nearly 50:50, is shown in Figure 3 (right). The *β*-SiC are comprised of repeating dark and white adjacent layers. That white layers represent the (111) planes which are clearly well arranged with the nearest neighboring planes of nearly 0.25 nm. This interplanar spacing is in an excellent agreement with *β*-SiC nanostructure with a particle size of 4 nm [33], *β*-SiC nanosphere having diameter of 30 nm [34], and *β*-SiC nanowires with 50 nm in diameter. The *d*-spacing corresponds to the XRD data using the Bragg angle of 35.7°. This fine-structured of nano *β*-SiC are promising for hydrogen production, in particular for the photocatalyst.

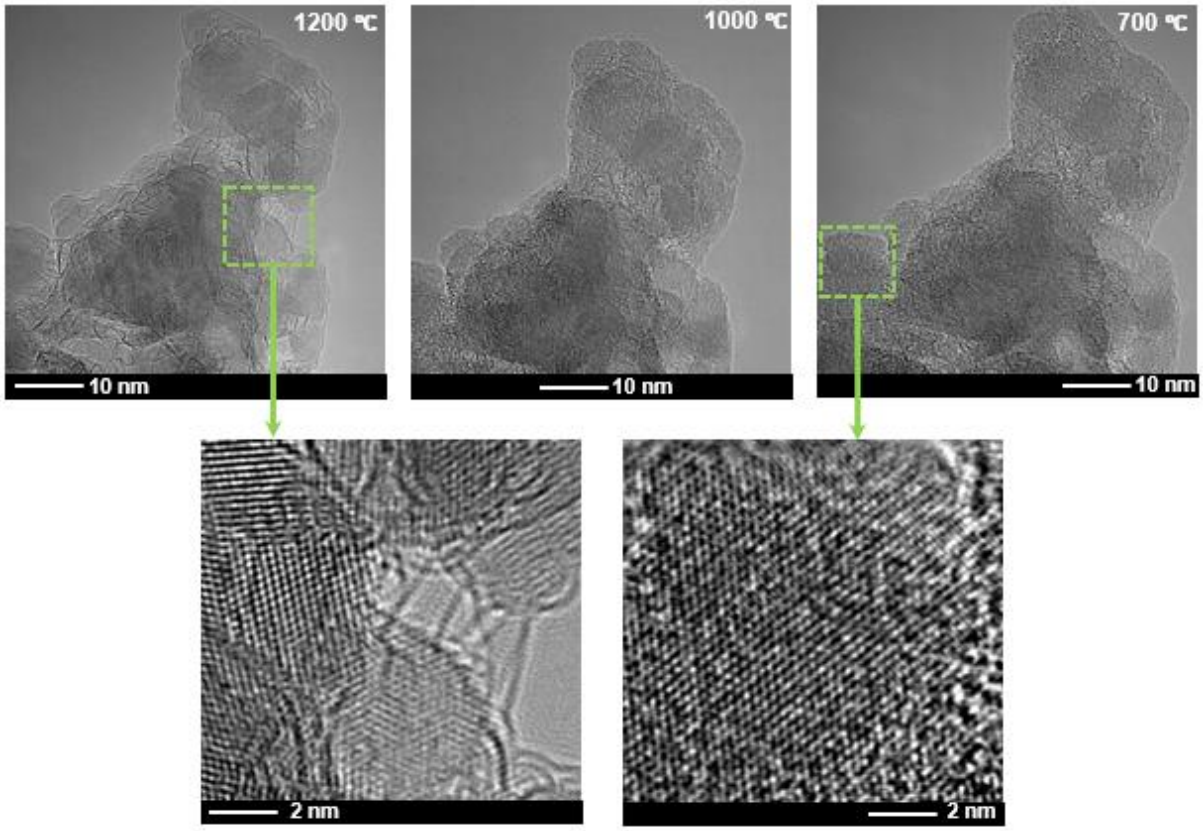

Figure 4. In-situ heating treatment using HR-TEM on the nanostructured β-SiC produced by magnesiothermic route.

The in-situ heating treatment using HRTEM reveals the evolution of ultra-fine sized β- SiC nanocrystals with good monodispersity, as can be observed from Figure 4. The average grain size of the β-SiC was approximately 6 nm, very close to the equivalent particle size extracted from the Rietveld method. The clear (111) crystalline planes can be again observed, after the digital zoom in view, of 700 °C and 1000 °C heat exposures. Unlike the well-aligned crystalline plane for T = 700 °C, some carbon layers appeared on β-SiC particles' surface at 1200 °C. Black carbon layers, by another study [35], were formed on β-SiC-(1 1 1) surfaces at 1360 °C and were confirmed by Raman scattering experiments. The growth of carbon nanotubes is located on the β-SiC nanoparticles' surface at [111] direction [36]. From this analysis, we may safely say that the carbon nanolayers are the manifestation of heating treatment of 1200 °C. Some carbon atoms started to diminish from the silicon-carbon strong chemical bond due to the thermal-driven external energy. These real-time evolutions can only be observed by the use of advanced HR-TEM. The tracing of this atomic-scale few changes is rather difficult to detect by powder XRD. Overall, the in-situ heating treatment by means of HRTEM clearly revealed the β-SiC crystalline state, as previously analyzed from XRD.

4. Conclusion

In this study, the detailed crystal structure investigations, from XRD to in-situ heat treatment HR-TEM, have been completed. On top of these successfully advanced measurements, the accomplishment of highly crystallized β-SiC was the half-success of the work. The beauty of crystal planes alignments, particularly in [111] direction, which corresponds to the highest XRD diffraction peak, within the cubic structured β-SiC nanoparticle was observed by HR-TEM image. In general, the in-situ HR-TEM dictated the fine crystalline state of β-SiC, including the presence of carbon nanolayers at a heating temperature of 1200 °C. These carbon nanolayers formation is a physical consequence of heating treatment at high

temperature. The STEM-EDS experiment revealed the proportionality of silicon and carbon atoms, with the values of respectively 47.1 at% and 52.9 at%. Last but not least, the fine structure of β-SiC is the key prior to being designed for any technological fields, including the hydrogen production application.

References

[1] Szczesny J, Marković N, Conzuelo F, Zacarias S, Pereira I A C, Lubitz W, Plumeré N, Schuhmann W and Ruff A 2018 A gas breathing hydrogen/air biofuel cell comprising a redox polymer/hydrogenase-based bioanode *Nat. Commun.* **9** 4715
[2] Kwon C H, Ko Y, Shin D, Kwon M, Park J, Bae W K, Lee S W and Cho J 2018 High-power hybrid biofuel cells using layer-by-layer assembled glucose oxidase-coated metallic cotton fibers *Nat. Commun.* **9** 4479
[3] Akella S H, D E, S S S R, Ahire A and Mal N K 2018 Studies on structure property relations of efficient decal substrates for industrial grade membrane electrode assembly development in pemfc *Sci. Rep.* **8** 12082
[4] Hidayat N, Istiqomah, Widianto M Y H, Taufiq A, Sunaryono, Triwikantoro, Zainuri M, Baqiya M A, Aristia G and S Pratapa 2017 Natural silica sand/alumina ceramic composites: promising candidates for fuel-cell sealants *IOP Conf. Ser. Mater. Sci. Eng.* **202** 012060
[5] Hidayat N, Triwikantoro, Baqiya M A and Pratapa S 2013 Thermal expansion coefficient prediction of fuel-cell seal materials from silica sand *AIP Conf. Proc.* **1555** 99–101
[6] Rezaei M, Salimi M, Momeni M and Mostafaeipour A 2018 Investigation of the socio-economic feasibility of installing wind turbines to produce hydrogen: Case study *Int. J. Hydrog. Energy*
[7] Zhou W, Yan L, Wang Y and Zhang Y 2006 SiC nanowires: A photocatalytic nanomaterial *Appl. Phys. Lett.* **89** 013105
[8] Hao J-Y, Wang Y-Y, Tong X-L, Jin G-Q and Guo X-Y 2012 Photocatalytic hydrogen production over modified SiC nanowires under visible light irradiation *Int. J. Hydrog. Energy* **37** 15038–44
[9] Zhou X, Gao Q, Li X, Liu Y, Zhang S, Fang Y and Li J 2015 Ultra-thin SiC layer covered graphene nanosheets as advanced photocatalysts for hydrogen evolution *J. Mater. Chem. A* **3** 10999–1005
[10] Wu R, Zhou K, Yue C Y, Wei J and Pan Y 2015 Recent progress in synthesis, properties and potential applications of SiC nanomaterials *Prog. Mater. Sci.* **72** 1–60
[11] Qteish A, Heine V and Needs R J 1993 Structural and electronic properties of SiC polytypes *Phys. B Condens. Matter* **185** 366–78
[12] Zhou J-Y, Chen Z-Y, Xu X-B, Zhou M, Ma Z-W, Zhao J-G, Li R-S and Xie E-Q 2010 Terbium-catalyzed selective area growth of SiC nanorods: synthesis, optimal growth, and field emission properties *J. Am. Ceram. Soc.* **93** 488–93
[13] Sundaresan S G, Davydov A V, Vaudin M D, Levin I, Maslar J E, Tian Y-L and Rao M V 2007 Growth of silicon carbide nanowires by a microwave heating-assisted physical vapor transport process using group VIII metal catalysts *Chem. Mater.* **19** 5531–7
[14] Kudrenko E, Roddatis V, Zhokhov A, Zverkova I, Khodos I and Emelchenko G 2012 Morphology of SiC nanowires grown on the surface of carbon fibers *RSC Adv.* **2** 4913–9
[15] Kamble M, Waman V, Mayabadi A, Funde A, Sathe V, Shripathi T, Pathan H and Jadkar S 2017 Synthesis of cubic nanocrystalline silicon carbide (3C-SiC) films by HW-CVD method *Silicon* **9** 421–9
[16] Lin H, Li H, Shen Q, Shi X, Feng T and Guo L 2018 3C-SiC Nanowires in-situ modified carbon/carbon composites and their effect on mechanical and thermal properties *Nanomaterials* **8** 894
[17] Qian B, Li H, Yang Z, Zhang Y, Su Y, Wei H and Zhang Y 2012 Inverted SiC nanoneedles grown on carbon fibers by a two-crucible method without catalyst *J. Cryst. Growth* **338** 6–11
[18] Nayak B B 2012 SiC/C nanocable structure produced in silicon carbide by arc plasma heating *Appl. Phys. A* **106** 99–104

[19] Yang X, Yang Z, Zhao S, Hu J and Luo X 2018 Synthesis of mesoporous Si/SiC with three-dimensional structure derived from C/silicalite-1 via magnesiothermic reduction *J. Porous Mater.* **25** 713–7
[20] Khan I, Saeed K and Khan I 2017 Nanoparticles: properties, applications and toxicities *Arab. J. Chem.* Article in-press.
[21] Fuad A, Mufti N, Diantoro M, Subakti and S. S K 2016 Synthesis and characterization of highly purified nanosilica from pyrophyllite ores *AIP Conf. Proc.* **1719** 030020
[22] Hunter B 1998 Rietica - A visual Rietveld program *Int. Union Crystallogr. Comm. Powder Diffr. Newsl. No. 20* (Summer) http://www.rietica.org
[23] Chen X, Zhang Q, Zhou Y, Qin Y, Liu X and Jia Q 2018 Synthesis of bamboo-like 3C-SiC nanowires with good luminescent property via nano-ZrO_2 catalyzed chemical vapor deposition technique *Ceram. Int.* **44** 22890–6
[24] Will G 2006 *Powder diffraction: the rietveld method and the two stage method to determine and refine crystal structures from powder diffraction data* (Springer Science & Business Media)
[25] Patterson A L 1939 The Scherrer formula for X-ray particle size determination *Phys. Rev.* **56** 978–82
[26] Wang F, Qin X, Zhu D, Meng Y, Yang L, Sun L and Ming Y 2015 $FeCl_2$-assisted synthesis and photoluminescence of β-SiC nanowires *Mater. Sci. Semicond. Process.* **29** 155–60
[27] Iwanowski R J, Fronc K, Paszkowicz W and Heinonen M 1999 XPS and XRD study of crystalline 3C-SiC grown by sublimation method *J. Alloys Compd.* **286** 143–7
[28] Palosz B, Grzanka E, Gierlotka S, Stel'makh S, Pielaszek R, Lojkowski W, Bismayer U, Neuefeind J, Weber H-P and Palosz W 2003 Application of X-ray powder diffraction to nanomaterials - determination of the atomic structure of nanocrystals with relaxed and strained surfaces *Phase Transit.* **76** 171–85
[29] Ortiz A L, Sánchez-Bajo F, Cumbrera F L and Guiberteau F 2013 The prolific polytypism of silicon carbide *J. Appl. Crystallogr.* **46** 242–7
[30] Peivaste I, Alahyarizadeh G, Minuchehr A and Aghaie M 2018 Comparative study on mechanical properties of three different SiC polytypes (3C, 4H and 6H) under high pressure: first-principle calculations *Vacuum* **154** 37–43
[31] Momma K and Izumi F 2011 VESTA 3 for three-dimensional visualization of crystal, volumetric and morphology data *J. Appl. Crystallogr.* **44** 1272–6
[32] Schardt J, Bernhardt J, Starke U and Heinz K 1998 Atomic structure of hexagonal 6H– and 3C–SiC surfaces *Surf. Rev. Lett.* **05** 181–6
[33] Yang S, Cai W, Zeng H and Xu X 2009 Ultra-fine β-SiC quantum dots fabricated by laser ablation in reactive liquid at room temperature and their violet emission *J. Mater. Chem.* **19** 7119–23
[34] Dasog M, Smith L F, Purkait T K and Veinot J G C 2013 Low temperature synthesis of silicon carbide nanomaterials using a solid-state method *Chem. Commun.* **49** 7004–6
[35] Watanabe H, Hisada Y, Mukainakano S and Tanaka N 2001 In situ observation of the initial growth process of carbon nanotubes by time-resolved high resolution transmission electron microscopy *J. Microsc.* **203** 40–6
[36] Kusunoki M, Rokkaku M and Suzuki T 1997 Epitaxial carbon nanotube film self-organized by sublimation decomposition of silicon carbide *Appl. Phys. Lett.* **71** 2620–2

Acknowledgments
This authors, especially N.H., would like to acknowledge Universitas Negeri Malang in providing a research fund, namely PPM-PNBP 2018.